Acta Crystallographica Section D
Biological Crystallography
ISSN 0907-4449

Crystallization of a nickel-containing superoxide dismutase and preliminary phase determination by MAD at the Ni *K* edge

Jochen Wuerges,[a,b] Jin-Won Lee,[c] Sa-Ouk Kang[c] and Kristina Djinovic Carugo[b]*

[a]International School For Advanced Studies, Via Beirut 2-4, I-34014 Trieste, Italy, [b]Structural Biology Laboratory, Sincrotrone Trieste in Area Science Park, S.S. 14 km 163.5, I-34012 Basovizza (TS), Italy, and [c]Laboratory of Biophysics, School of Biological Sciences, and Institute of Microbiology, Seoul National University, Seoul 151-742, South Korea

Correspondence e-mail: djinovic@elettra.trieste.it

Received 9 January 2002
Accepted 22 April 2002

Superoxide dismutases are metalloenzymes which catalyse the disproportion of superoxide radicals and thus play an important role in the protection of biomolecules from oxidative damage. Redox-active metal ions known to act as the catalytic centre of these enzymes are Cu, Mn or Fe. Recently, enzymes containing Ni have been found in various *Streptomyces* species, introducing a fourth type of metal ion to the superoxide dismutase family. NiSOD has been crystallized for the purpose of structure determination by X-ray crystallography using Ni as an anomalous scatterer in multiple-wavelength anomalous dispersion (MAD) experiments. Two crystal forms belonging to space group $P2_12_12_1$ and one belonging to space group $R3$ were obtained using ammonium sulfate as a precipitant. Patterson maps of one of the orthorhombic forms revealed the presence of pseudo-translation, which could be removed for the other orthorhombic form by using 10% glycerol in its crystallization conditions. In addition, this reduced the unit cell by half. Phase information which led to interpretable electron-density maps was derived from MAD data to 2.0 Å resolution after density modification applying solvent flattening, histogram matching and NCS averaging. Phases were extended to 1.68 Å resolution with a data set collected at a wavelength of 1 Å. Model building based on the resulting electron-density maps is in progress.

1. Introduction

Superoxide dismutases (SODs; EC 1.15.1.1) are almost ubiquitous metalloenzymes which dismute the superoxide radical anion ($O_2^{\cdot-}$) to molecular oxygen (O_2) and peroxide (H_2O_2). They are important for the protection of biological molecules from oxidative damage caused either by the superoxide radical itself or by its reactive products. In oxygen-metabolizing organisms, $O_2^{\cdot-}$ is generated as an intermediate by a single electron transfer to molecular oxygen during its reduction to H_2O, but is also generated to a substantial amount by a number of enzymes (Fridovich, 1998). Superoxide dismutases are generally classified according to the metal species which acts as the redox-active centre in these enzymes. Until recently, three different metal species have been found. Copper- and zinc-containing SOD (Cu,ZnSOD), with copper as the catalytically active metal, and manganese-containing SOD (MnSOD) have been isolated both from prokaryotes and eukaryotes, including mammals (McCord & Fridovich, 1969). Iron-containing SOD (FeSOD) has been found in prokaryotes, such as *Escherichia coli* (Yost & Fridovich, 1973), in primitive eukaryotes and in plants. More recently, two new superoxide dismutases have been purified from a variety of *Streptomyces* species (Youn, Kim *et al.*, 1996; Youn, Youn *et al.*, 1996; Kim *et al.*, 1996). These are iron- and zinc-containing SOD (Fe,ZnSOD) and nickel-containing SOD (NiSOD), the latter introducing a novel class of SODs. The dissimilarity of NiSOD to other members of the SOD families is likely to extend beyond the metal type in the catalytically active site, as its amino-acid sequence revealed no homology to the amino-acid sequences of other SODs. It is therefore expected that NiSOD represents a new class of SODs not only with respect to the catalytic metal type but also with respect to its three-dimensional structure. The determination of the metal contents indicated one nickel ion per monomer (Youn, Kim *et al.*, 1996). Kinetic and spectroscopic studies of NiSOD show that its catalytic activity is of the same high level as that of Cu,ZnSOD, while the metal-coordination environment differs greatly from all other members of the SOD classes in that it contains thiolate ligands (Choudhury *et al.*, 1999).

An X-ray crystallographic study has been carried out to obtain insight into the enzyme's overall architecture and the structure of the active site in particular. In addition, this information may contribute to the general

understanding of catalytic mechanisms performed by nickel-containing enzymes, of which only a small number are known at the molecular level. Examples of structurally known nickel-containing enzymes, all of which were reviewed in Maroney (1999), include urease as a hydrolytic enzyme and [NiFe]-hydrogenase, carbon monoxide dehydrogenase and methyl coenzyme M reductase as redox-active enzymes. Here, we report on the crystallization and preliminary crystallographic analysis of the enzyme NiSOD from *Streptomyces seoulensis* (Chun *et al.*, 1997).

2. Materials and methods

2.1. Protein purification

The sample of NiSOD was obtained as described previously (Youn, Kim *et al.*, 1996). The oligomerization state of NiSOD was reported previously as a tetramer (Youn, Kim *et al.*, 1996); however, further investigation by mass spectrometry, analytical ultracentrifugation and heterologous expression test revealed NiSOD to be a hexamer (unpublished data). Protein was stored in buffer *A* (50 m*M* sodium phosphate pH 7.4) and 30% glycerol at a concentration of 40 mg ml^{-1}. Further purification prior to use in crystallization trials was performed on a Superdex 200 column.

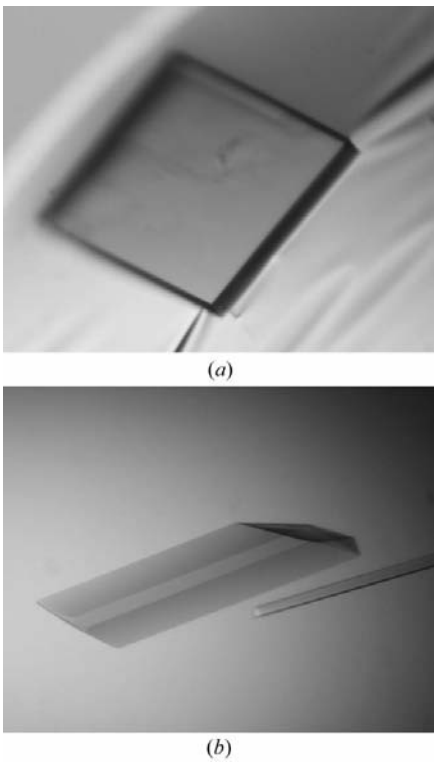

Figure 1
(*a*) Crystal form I of NiSOD, orthorhombic lattice, with dimensions of approximately 0.21 × 0.21 × 0.04 mm. (*b*) Crystal of form II (macroseeded needle-shaped crystal to the right, rhombohedral lattice) and of form III (rod-shaped crystal at the centre, orthorhombic lattice). This rod crystal grew 5–6 weeks after macroseeding the needle to the drop shown here.

2.2. Crystallization

For crystallization, the buffer was exchanged to 50 m*M* NaCl and 20 m*M* Tris pH 8.0 (all chemicals from Fluka) by serial washing in a Centricon (Amicon) and was concentrated to 10.6 mg ml^{-1}. Crystallization trials were carried out by the hanging-drop vapour-diffusion method (McPherson, 1999) at 277 and 293 K. Initial screens utilized premixed conditions (Jancarik & Kim, 1991) which were refined to improve crystal growth. NiSOD crystallizes in more than one form and in the following only those crystal forms which exhibited high quality in X-ray diffraction experiments are described. 1 µl of protein solution was mixed with 1 µl of crystallization reagent and the plates were stored at 293 K.

2.2.1. Crystal form I. The first crystals of NiSOD grew readily from a premixed crystallization reagent (purchased from Hampton Research) consisting of 2 *M* ammonium sulfate and 5% 2-propanol. The small amount of 2-propanol proved to be necessary for crystal growth. The pH of this condition is 5.25. Plate-like crystals with approximate dimensions of 0.21 × 0.21 × 0.05 mm appeared after 1–2 weeks (Fig. 1*a*).

2.2.2. Crystal form II. Needle-shaped crystals were obtained after 8–10 d from 1.85 *M* ammonium sulfate and 0.1 *M* sodium acetate pH 5.25, showing an approximate length of 0.3 mm and a diameter of 0.03 mm (Fig. 1*b*). Macroseeding (Thaller *et al.*, 1981) these needle crystals to crystallization drops containing 1 µl of 1.78 *M* ammonium sulfate, 0.1 *M* sodium acetate and 1 µl fresh protein solution was tried to attempt to increase the crystal size. No significant crystal growth could be observed, but instead a new crystal form III appeared after 5–6 weeks in the macroseeding drops, showing a different morphology and space group (see §2.2.3).

2.2.3. Crystal form III. Rod-like crystals with typical dimensions of approximately 0.5 × 0.2 × 0.2 mm (Fig. 1*b*) were first obtained as a byproduct of macroseeding form II crystals as described above. Growth of form III crystals in this manner was reproducible, but more convenient growth conditions were found to be 1.85 *M* ammonium sulfate, 0.1 *M* sodium acetate pH 5.25 and 10% glycerol, from which crystals grew in 5–6 weeks.

Table 1
The three NiSOD crystal forms.

Crystal form	Form I	Form II	Form III
X-ray source	ESRF, BM14	EMBL c/o DESY, BW7A	ESRF, ID14-4
Space group	$P2_12_12_1$	$R3$	$P2_12_12_1$
Unit-cell parameters (Å)			
a	112.3	189.4	65.2
b	113.8	189.4	119.3
c	128.6	159.9	121.0
No. of molecules per AU†	12	18	6
V_M† (Å^3 Da^{-1})	2.6	2.3	3.0
Solvent content† (%)	51	46	57

† Using the molecular mass of NiSOD of 13.2 kDa and a molecular-density value of 1.3 g cm^{-3} to estimate the solvent content of the crystals (Matthews, 1968).

2.3. X-ray data collection and processing

Multiple-wavelength anomalous dispersion (MAD) data sets were collected from cryocooled (100 K) crystals of each of the three crystal forms at the Ni *K* edge. Cryoprotectant solutions consisted of the respective crystallization conditions with the addition of 20%(*v*/*v*) glycerol. Crystal characteristics are summarized in Table 1. The choice of space group for crystal forms I and III as $P2_12_12_1$ was made on the basis of systematic absences of axial reflections with uneven indices and, noting the small difference in two of the unit-cell parameters, by much poorer merging statistics when the crystal was treated as tetragonal.

The X-ray fluorescence spectra at the Ni *K* edge were measured before each MAD data collection, which consisted of a peak, inflection-point and high-energy remote data set. From the fluorescence spectra, anomalous scattering factors f' and f'' were calculated with the program *CHOOCH* (Evans & Pettifer, 2001) to select suitable X-ray energy values for data collection. Plots of f' and f'' about the theoretical absorption edge energy of 8333 eV show a broad dip in f' with a minimum of −7.7 and a maximum f'' of 4.3 without a white-line feature in both the resting state (Ni^{III}) and the thiosulfate-reduced state (Ni^{II}).

MAD data-processing and reduction statistics are given in Table 2. The program *DENZO* (Otwinowski & Minor, 1997) and, for post-refinement of unit-cell parameters, *SCALEPACK* (Otwinowski & Minor, 1997) were used as well as *MOSFLM* (Leslie, 1992) for data processing and *SCALA* (Collaborative Computational Project, Number 4, 1994) for data reduction, applying a MAD data-specific scaling

Table 2
Processing and reduction statistics of MAD data sets for crystal forms I and III.

MAD data set†	Wavelength (Å)	Resolution range (Å)	Completeness‡ (%)	R_{anom}§ (%)	$\langle I/\sigma(I)\rangle$‡	R_{sym}¶‡ (%)	Redundancy
Form I		31.1–2.2					
Pk	1.4827		99.7 (99.7)	4.2	11.9 (3.3)	5.6 (18.7)	4.7
Pi	1.4859		99.5 (99.5)	4.1	11.3 (3.4)	6.2 (22.4)	4.6
Re	1.2398		99.8 (98.7)	3.3	13.3 (5.5)	4.8 (13.6)	4.6
Form III		44.0–2.0					
Pk	1.4863		98.6 (98.6)	3.2	9.3 (2.2)	5.2 (21.7)	6.3
Pi	1.4756		98.5 (97.0)	2.9	6.7 (1.9)	6.2 (27.5)	6.3
Re	0.9392		99.2 (98.5)	2.4	6.3 (2.8)	7.5 (20.9)	8.0

Statistics of data to higher resolution than for the corresponding MAD data.

High-resolution data sets	Wavelength (Å)	X-ray source	Resolution range (Å)	Completeness†† (%)	$\langle I/\sigma(I)\rangle$††	R_{sym}¶†† (%)	Redundancy
Form I	0.9326	ESRF, ID14-2	42.6–1.6	98.9 (97.6)	13 (2.8)	8.0 (26.0)	3.7
Form III	1.0	ELETTRA, XRD1	34.3–1.68	99.1 (96.0)	11 (2.1)	4.3 (27.6)	6.6

† Pk, peak-energy; Pi, inflection-point; Re, remote-energy data. ‡ Values in parentheses are for the outer resolution shell, 2.32–2.2 Å (form I), 2.11–2.0 Å (form III). § $R_{anom} = \sum_{hkl} |I_+ - I_-| / \sum_{hkl} |I_+ + I_-|$. ¶ $R_{sym} = \sum_{hkl} \sum_i |I_i - \langle I\rangle| / \sum_{hkl} \sum_i |I_i|$. ††Values in parentheses are for the outer resolution shell: 1.69–1.6 Å (form I), 1.76–1.68 Å (form III).

protocol. The R factors for merging the three subsets of MAD data were 6.9 and 8.7% for forms I and III, respectively. Structure-factor amplitudes were obtained from the intensities using *TRUNCATE* and were further analysed by *SCALEIT*, both of which are from the Collaborative Computational Project, Number 4 (1994).

Diffraction data to higher resolution than that of the respective MAD data were subsequently collected for both the orthorhombic crystal forms I (to 1.6 Å) and III (1.68 Å). Processing and reduction statistics using *MOSFLM* and *SCALA* are compiled in Table 2.

3. Patterson analysis and determination of initial phases

3.1. Crystal form I

Native as well as anomalous and dispersive difference Patterson maps were calculated for the MAD data described in Table 2 using the program suite *CNS* (Brünger *et al.*, 1998). All maps showed an outstanding peak (20% of the origin-peak height) at $u = 0.05$, $w = 0$ in the $v = \frac{1}{2}$ Harker section. This peak indicated the presence of pseudo-translation. which is a special type of non-crystallographic symmetry (NCS). The heavy-atom partial structure was solved using automated Patterson methods as implemented in *CNS* and *SOLVE* (Terwilliger & Berendzen, 1999). Both programs found the same 12 sites per asymmetric unit. The correctness of these sites was confirmed by inspection of anomalous difference Fourier and log-likelihood gradient maps in the graphics program *O* (Jones *et al.*, 1991) after MAD phasing with only nine sites chosen randomly from the 12 peaks. The omitted sites were clearly visible as the highest peaks in the log-likelihood gradient map. The nickel sites are arranged in two identical spatially separated groups, each forming a slightly distorted octahedron with distances between Ni-positions along edges ranging from 23.4 to 27.7 Å. This indicates that the oligomerization state is a hexamer also in the crystalline state.

The pseudo-translation vector (0.05, 0.5, 0) or $a/20 + b/2$, as concluded from Patterson maps, was inserted into the structure-factor defining equation to derive both the effect of this purely translational NCS on the structure factors $\mathbf{F}(hkl)$ and the parity groups of reflections for which a certain modulation of $\mathbf{F}(hkl)$ holds. For the parity group ($h = 20n$, $k = 2n$), where n is an integer, no modulation of the structure factor exists, *i.e.* the observed $\mathbf{F}(hkl)$ equals that in the case of absent pseudo-translation. In the 1.6 Å data set, only 2.9% of the unique reflections belong to this group. All other parity groups show modulation of the magnitude of $\mathbf{F}(hkl)$ and, where the integer m in $h = 20n + m$ equals one of the values $1, \ldots, 9, 11, \ldots, 19$, the phase of $\mathbf{F}(hkl)$ is also affected. The pseudo-translation was characterized in the manner proposed by Chook *et al.* (1998). The ratio of the averaged structure factor in case of absent modulation to the averaged structure factor for a given parity group with modulations is used as a quantitative indicator for the presence of pseudo-translation. Values of this ratio that deviate from 1 by more than 20% are taken as a criterion of this kind of NCS. The averaged structure factors in resolution bins were calculated for the purpose of this analysis with *TRUNCATE* simply as the square root of the observed intensities. The expected modulations occur in an attenuated form for reflections in the lower resolution bins (<3 Å), *i.e.* as systematic weakness of intensities rather than extinction or as a small increase where a doubled structure-factor amplitude is expected.

The figure of merit (FOM) of initial phases calculated by *CNS* with data to 2.4 Å resolution was 0.6. Electron-density maps were not interpretable in any region of the asymmetric unit, despite the promising FOM. After solvent flipping as implemented in *CNS* the protein boundary was visible; however, the electron density within the protein region remained uninterpretable. The pseudo-translation has until now been considered in phase calculations only in NCS averaging of pseudo-translationally related electron-density regions. The improvement was negligible, even though the correlation between averaged density was 0.8 (see discussion in §4).

3.2. Crystal form III

Native Patterson maps did not indicate the presence of pseudo-translation as observed for crystal form I. Together with the observation that the unit cell is reduced by half with respect to form I, it is evident that pseudo-translational NCS in form I crystals has turned into crystallographic symmetry in case of crystal form III. Solution of the heavy-atom partial structure was performed as described in §3.1. The six nickel-ion positions per asymmetric unit showed the same distorted octahedron as seen in both hexameric arrangements in the form I asymmetric unit. Most probably as a consequence of radiation damage, which became significant during collection of the remote-energy data, which was the last data set taken, better maps were obtained when the remote-energy data were omitted from local scaling and phase calculation. With peak and inflection-point data sets alone, an overall FOM of 0.52 was obtained when reflections to 2.8 Å were used (0.57 with data to 2.0 Å). Electron-density maps after solvent flipping provided six α-helical partial structures which were modelled with the program *O*. Utilizing the nickel ions as reference points, it was evident that every partial structure represented the same patch in each of the six subunits, thus allowing the use of these partial models for determination of NCS operators. These operators were

used in the program *DM* (Cowtan, 1994) for NCS averaging. The subunit mask was determined automatically by the program and improved, together with the NCS operators, in the first run. In subsequent runs, the improved phases, subunit mask and NCS operators were used iteratively, reaching a correlation coefficient of 0.81. At this stage, the electron-density map was interpretable in almost all parts of the protein. Further phase refinement and extension to 1.68 Å resolution of the additionally collected data set was performed with the program suite *ARP/wARP* (Perrakis *et al.*, 1997).

4. Results and discussion

Crystals of the enzyme NiSOD could be grown from various conditions. All crystals of sufficient quality for X-ray diffraction data collection, however, grew at the same pH of 5.25 and from almost equal concentrations of ammonium sulfate as precipitant. The coexistence of the rhombohedral crystal form II and the orthorhombic crystal form III inside the same crystallization drop during macroseeding experiments illustrates this close relationship. The crystallization conditions for the three crystal forms described here are similar with respect to their chemical composition, but gave rise to considerably differing unit-cell parameters and numbers of molecules per asymmetric unit (Table 1). Along the crystallographic axes *a* and *b*, form I shows similar unit-cell parameters to form III along axes *b* and *c*, respectively, whereas the *c* axis of form I is nearly twice as long as the *a* axis of form III. The resultant reduction of the form I unit cell by half is accompanied by a reduction of the number of molecules per asymmetric unit from 12 to six as found in form III. Both crystal forms grew from ammonium sulfate as precipitant at similar molarity but differ in the type of organic additive: 2-propanol in the case of form I crystals and glycerol in the case of form III crystals. Glycerol may modify the hydration state of the protein (Sousa & Lafer, 1990), allowing the crystal contacts that are responsible for the arrangement of molecules in the smaller unit cell.

The second and more important effect of the molecular rearrangement that resulted in crystal form III has been the removal of the pseudo-translation which relates two hexamers in crystal form I by the vector (0.05, 0.5, 0). Characterization of this special type of NCS by ratios of averaged structure factors for certain parity groups revealed that low-resolution reflections are affected by modulations of the structure-factor magnitude and, for many parity groups, of the phase angle as well. MAD phasing with this crystal form could not be performed successfully, as no procedure for calculation of protein phase angles which could appropriately take into account the observed structure-factor modulations is implemented in available macromolecular crystallography program packages. NCS averaging of the translationally related hexamers did not improve the quality of electron-density maps. The explanation might be that there is only little additional information gained for phase improvement by averaging two density regions in an asymmetric unit if the NCS *almost* equals a crystallographic symmetry that would force the two regions to be in separate unit cells. This crystallographic situation is realised in crystal form III, where a hexamer-relating translation corresponding to the 0.05 component of the pseudo-translation vector is not present. Thus, a purely crystallographic translation along the axis corresponding to the *b* axis of form I is possible and leads to the observed splitting of the unit cell. It is therefore the small but important component of 0.05 which does not permit the solution of the pseudo-translation problem by the introduction of pseudo-origins. This could correct for the component of 0.5 along *b* if it was present as the only component of pseudo-translation (see, for example, Morais *et al.*, 2000, for a successful treatment of this case of a pseudo-translation vector).

Interpretable electron-density maps of NiSOD were obtained using the peak and inflection-point data to 2.0 Å resolution of a MAD experiment on crystal form III. One nickel ion per subunit (117 amino acids, 13.2 kDa) could be successfully used as anomalous scatterer for MAD phasing. The nickel sites of a hexamer form a distorted octahedron-like arrangement which shows one threefold NCS axis and three twofold axes perpendicular to the threefold. Initial phases were improved by solvent flattening, histogram matching and averaging the density of six NCS related molecules per asymmetric unit to permit an almost complete interpretation of the electron density. Subsequently, phases have been extended to 1.68 Å and interpretation of the resulting electron-density map is currently in progress.

We wish to thank Gordon Leonard, Edward Mitchell and Andy Thompson at ESRF, and Paul Tucker at EMBL c/o DESY for help during data collection and also Gordon Leonard for help during initial MAD data analysis. Many thanks to Paul Adams, Clemens Vonrhein, Gérard Bricogne and Eleanor Dodson for helpful discussions about phasing and pseudo-translation.

References

Brünger, A. T., Adams, P. D., Clore, G. M., DeLano, W. L., Gros, P., Grosse-Kunstleve, R. W., Jiang, J.-S., Kuszewski, J., Nilges, M., Pannu, N. S., Read, R. J., Rice, L. M., Simonson, T. & Warren, G. L. (1998). *Acta Cryst.* D**54**, 905–921.

Chook, Y. M., Lipscomb, W. N. & Ke, H. (1998). *Acta Cryst.* D**54**, 822–827.

Choudhury, S. B., Lee, J.-W., Davidson, G., Yim, Y.-I., Bose, K., Sharma, M. L., Kang, S.-O., Cabelli, D. E. & Maroney, M. J. (1999). *Biochemistry*, **38**, 3744–3752.

Chun, J., Youn, H.-D., Yim, Y.-I., Lee, H., Kim, M. Y., Hah, Y. C. & Kang, S.-O. (1997). *Int. J. Syst. Bacteriol.* **47**, 492–498.

Collaborative Computational Project, Number 4 (1994). *Acta Cryst.* D**50**, 760–763.

Cowtan, K. (1994). *Jnt CCP4/ESF–EACMB Newsl. Protein Crystallogr.* **31**, 34–38.

Evans, G. & Pettifer, R. F. (2001). *J. Appl. Cryst.* **34**, 82–86.

Fridovich, I. (1998). *Oxidative Stress*. In *Encyclopedia of Life Sciences*, http://www.els.net.

Jancarik, J. & Kim, S.-H. (1991). *J. Appl. Cryst.* **24**, 409–411.

Jones, T. A., Zou, J. Y., Cowan, S. W. & Kjeldgaard, M. (1991). *Acta Cryst.* A**47**, 110–119.

Kim, E.-J., Kim, H.-P., Hah, Y. C. & Roe, J.-H. (1996). *Eur. J. Biochem.* **241**, 178–185.

Leslie, A. G. W. (1992). *Jnt CCP4/ESF–EACMB Newsl. Protein Crystallogr.* **26**.

McCord, J. M. & Fridovich, I. (1969). *J. Biol. Chem.* **244**, 6049–6055.

McPherson, A. J. (1999). *Crystallization of Biological Macromolecules*. New York: Cold Spring Harbor Laboratory Press.

Maroney, M. J. (1999). *Curr. Opin. Chem. Biol.* **3**, 188–199.

Matthews, B. W. (1968). *J. Mol. Biol.* **33**, 491–497.

Morais, M. C., Baker, A. S., Dunaway-Mariano, D. & Allen, K. N. (2000). *Acta Cryst.* D**56**, 206–209.

Otwinowski, Z. & Minor, W. (1997). *Methods Enzymol.* **276**, 307–326.

Perrakis, A., Sixma, T. K., Wilson, K. S. & Lamzin, V. S. (1997). *Acta Cryst.* D**53**, 448–455.

Sousa, R. & Lafer, E. M. (1990). *Methods*, **1**, 50–56.

Thaller, C, Weaver, L. H., Wilson, E., Karlsson, R. & Jansonius, J. N. (1981). *J. Mol. Biol.* **147**, 465–469.

Terwilliger, T. C. & Berendzen, J. (1999). *Acta Cryst.* D**55**, 849–861.

Yost, F. T. & Fridovich, I. (1973). *J. Biol. Chem.* **248**, 4905–4908.

Youn, H.-D., Kim, E.-J., Roe, J.-H., Hah, Y. C. & Kang, S.-O. (1996). *Biochem J.* **318**, 889–896.

Youn, H.-D., Youn, H., Lee, J.-W., Yim, Y.-I., Lee, J. K., Hah, Y. C. & Kang, S.-O. (1996). *Arch. Biochem. Biophys.* **334**, 341–348.